Layer structure formation in oriented poly(ethylene terephthalate) relating to micromechanical properties

T. Uchiyama[a], M. Suyama[a], M. M. Alam[a] , T. Asano[a*],
S. Henning[b], A. Flores [c], F. J. Baltá Calleja [c], M. F. Mina[d]

[a]*Materials Science, Graduate School of Science and Engineering, Shizuoka University, Ohya 836, 422-8529, Shizuoka, Japan*

[b]*Department of Engineering, Institute of Materials Science, Martin-Luther-Universität Halle-Wittenberg, D-06099 Halle/Saale, Germany*

[c]*Instituto de Estructura de la Materia, CSIC, Serrano 119, 28006 Madrid, Spain*

[d]*INST, Atomic Energy Research Establishment, GPO Box 3787, Dhaka-1000, Bangladesh*

Abstract

Glassy poly(ethylene terephthalate), uniaxially drawn at 25°C (cold-drawing) and at 90°C (hot-drawing), was crystallized in a taut state without shrinkage at 100°C, 150°C, 200°C and 250°C. The nanostructure and the mechanical properties were surveyed by x-ray diffraction and microhardness. Small angle x-ray diffraction diagrams reveal typical 4-point patterns characteristic of the cold-drawn samples, whereas 2-point patterns are observed for the hot-drawn ones. Comparison of the molecular and the nanolayer inclinations in both drawings suggests that a mutual supplementary relationship holds between the *c*-axis tilting and the lamellar inclination. The layer structure formation is discussed in the light of these results. In addition, a correlation between the nanostructure formation and the micromechanical properties is offered, highlighting the differences found between the hot- and the cold-drawn material.

Key Words: Poly(ethylene terephthalate), x–ray diffraction, Microhardness
*Corresponding author. Tel: +81-54-238-4743; fax: +81-54-238-4743.
E-mail address: sptasan@sci.shizuoka.ac.jp

1. Introduction

Glassy poly(ethylene terephthalate) (PET) can be drawn through neck formation at room temperature. The drawn material is highly oriented, however it does not exhibit any crystalline order [1]. A gradual increase of the degree of order can be achieved by means of annealing [2]. Bonart was the first researcher to observe the structural transformation taking place upon mechanical drawing of PET, from a totally amorphous into a nematic- and, finally, to a smectic state [3]. Yeh and Geil demonstrated using electron microscopy that glassy PET is composed of spherical-like structures in which the molecules exhibit a paracrystalline order [4]. The mechanism of transformation from the glassy nematic state to the smectic phase, and finally into the triclinic structure has been the subject of a number of investigations and is still a matter of debate [5-9].

Morphological studies on the primary crystallization of drawn PET have been performed by several authors [10-14]. Triclinic PET sometimes reveals a unique tilted-orientation (the -230 orientation), which was first reported by Daubeny et al [15]. Asano and Seto later studied in detail the dependence of the tilted-orientation on the annealing temperature [2]. In addition, cold-drawn PET may also exhibit a lamellar inclination that seems to diminish as the annealing temperature increases [5].

For cold-drawn PET, we discussed the role of the molecular axis tilting and the lamellar inclination on the mechanism of the smectic to triclinic transformation [5]. Starting from the smectic state, molecular and layer inclinations are necessary to produce the required density difference between the amorphous and crystalline layers. In addition, microindentation hardness was used to distinguish between the oriented glassy samples, the smectic phase and the crystalline nanofibrils. These microhardness studies provided valuable information on the mechanical behaviour of the semicrystalline fibrils, with special reference to the amorphous intercrystalline layers. It is well known that microindentation hardness is a powerful technique capable of detecting a variety of morphological and nanostructural changes in polymers [16], especially PET [17-22].

In the present work, we wish to examine the crystallization mechanism taking place in glassy PET, hot-drawn above the glass the transition temperature (T_g = 69°C) without neck formation, as compared to the cold-drawn material. The morphological changes occurring after annealing at temperatures, T_a, above T_g and up to 250 °C have been followed by x-ray diffraction and microindentation hardness measurements. The mechanism of nanolayer structure formation upon crystallization is discussed, with special emphasis into the process of molecular and layer inclinations. Finally, the nanostructure-micromechanical properties correlation is highlighted.

2. Experimental

2.1. Materials

Amorphous PET (M_n = 18000 g/mol) from Toray Co. Ltd. Japan was used in this study. Isotropic films having a thickness of 0.72 mm were uniaxially drawn using a Tensilon UTM 4-100, Toyo Boldwin Co. Ltd. The cold-drawing process was carried out at room temperature (25 °C) using a drawing speed of 4.0 mm/min. On the other hand, hot-drawing was performed at 90 °C with a drawing speed of 35.2 mm/min. The draw ratio was approximately 4 in both hot- and cold-drawing processes. The films slightly whitened after the uniaxial drawing, the final thickness being of ~ 0.30–0.33 mm.

Figure 1 illustrates the coordinates for the drawn sample, where the Z-axis is parallel to the drawing direction. X- and Y-axes are perpendicular and parallel to the film surface, respectively. Portions of the drawn samples (40 mm in length and 3 mm in width) were annealed in an oven at 100 °C, 150 °C, 200 °C and 250 °C for 10^4 s. The sample ends were clamped during the annealing process to fix the sample length.

2.2. Density measurements

The density values of the annealed PET samples are collected in Table 1 and were measured by the floating method described in reference 5. The volume degree of crystallinity, α, was derived from the density ρ following:

$$\alpha = (\rho - \rho_a) / (\rho_c - \rho_a) \quad (1)$$

where ρ_c and ρ_a are the densities of the crystalline and amorphous phases, respectively. The amorphous density of the drawn PET material is taken to be 1.37 g/cm^3, which is the measured density of the cold-drawn amorphous sample [5]. The density of the triclinic crystal is assumed to be ρ_c = 1.455 g/cm^3 [15].

2.3. X-ray Diffraction

The 2-D wide angle (WAXS) and small angle x-ray diffraction (SAXS) patterns were recorded using a high-intensity x-ray generator (Rigaku RU300). The imaging plate of Fuji Photo Film Co. Ltd. was placed at a distance from the sample of 54 mm and 434 mm for WAXS and SAXS measurements, respectively. The incident x-ray beam was monochromized using a graphite single crystal (λ = 1.54 Å). A point slit of 100 μm in diameter was used for collimation purposes.

The x-ray diffraction patterns were recorded with three different incident directions as shown in Figure 1; i) parallel to the X-axis ("through" patterns), ii) parallel to the Y-axis ("edge" patterns) and iii) parallel to the Z-axis (end patterns).

2.4. Microindentation hardness

Microhardness experiments were carried out at room temperature using a Leica Microsystems indentation equipment. A Vickers square-based diamond pyramid was used. Microhardness values, H, are calculated following;

$$H = k\,P/d^2 \tag{2}$$

where P is the load applied, d is the measured diagonal of the residual impression and k is a geometric constant. A value of $k = 1.854$ is used when P is in N and d in mm to give H in MPa. A load of 0.98 N was applied for 6 s to minimize the creep of the sample under the indenter [16]. The P/d^2 ratio was observed to be constant for different loads.

The sample was positioned with the drawing axis parallel to one of the indentation diagonals. Owing to sample orientation, the residual impression shows anisometric diagonal lengths. We define H_{II} and $H_{\perp}$ as the hardness values derived from the diagonal lengths parallel and perpendicular to the drawing direction respectively. The indentation anisotropy, ΔH, is defined as [16];

$$\Delta H = 1 - (H_{\perp}/H_{\text{II}}) \tag{3}$$

$H_{\perp}$ is related to the plastic deformation mode of the lamellar stacks. On the other hand, the larger H_{II} values arise from the instant elastic recovery of the material in the drawing direction after load release [5]. The indentation anisotropy is a consequence of the orientation of the molecular axis, giving rise to a larger elastic recovery of the material in the chain direction. It has been shown that ΔH is a suitable parameter for measuring the preferred chain axis orientation [16]. Indeed, a linear empirical correlation has been found between ΔH and the optical birefringence Δn for injection-moulded oriented polyethylene [16].

In addition, the hardness of a polymeric material is well described by a parallel model of alternating amorphous and crystalline regions, with hardness values H_a and H_c respectively [16]:

$$H = H_c\,\alpha + H_a\,(1-\alpha) \tag{4}$$

where α is the volume degree of crystallinity. Moreover, H_c is related to the crystalline lamellar thickness, l_c, through [16];

$$H_c = \frac{H_c^{\infty}}{1 + \frac{b}{l_c}} \tag{5}$$

where H_c^{∞} is the hardness of an infinitely thick crystal and b is a parameter defined as:

$$b = 2\sigma_e/\Delta h \tag{6}$$

σ_e being the surface free energy of the crystals and Δh the energy required for plastic deformation of the crystalline lamellae.

3. Results and discussion

3.1. Layer structure formation studied by x-ray diffraction

3.1.1. WAXS measurements at room temperature: hot- versus cold-drawing

Figure 2a illustrates the WAXS pattern of the cold- (left-hand side) and of the hot- (right-hand side) drawn PET sample before annealing. Figure 2b shows the plot of the intensity distribution at $2\theta = 20 \pm 2$ ° as a function of the azimuthal angle (the Z-axis is the origin of the azimuthal angle values), for both, hot and cold-drawing. For cold-drawn PET, two strong equatorial maxima can be clearly distinguished in Figure 2a, together with several layer lines on the meridian and no trace of crystalline reflections. The meridional maxima can be associated to the highly oriented nematic-like molecule [23]. In contrast, the WAXS pattern of hot-drawn PET displays a diffuse broad ring with a slightly higher intensity around the equator. No significant crystallinity is observed, however, initiation of crystallization cannot be discarded as the drawing process was carried out above T_g. Figure 2b shows two maxima in the intensity distribution at 90 ° and 270 ° for both drawing

processes, however, the peaks are broader and the maximum intensity is substantially smaller for the hot-drawn sample. The above results suggest that cold-drawn PET exhibits a nematic-like structure where the molecules are preferentially arranged parallel to the drawing direction. In contrast, molecules in the hot-drawn sample are poorly oriented along the drawing axis, i.e, the chain direction exhibits a wide distribution with respect to the Z-axis.

3.1.2. Nanostructure development in cold-drawn PET: comparison of "through" versus "edge" directions

The WAXS patterns for cold-drawn PET annealed at various T_a are shown in Figure 3, both in the "through" (left-hand side) and "edge" (right-hand side) arrangements. It is noteworthy that the reflection maxima become more intense and sharper as the annealing temperature is raised. This suggests that not only the degree of crystallinity increases with increasing annealing temperature (see Table 1), but in addition, the degree of perfection of the triclinic crystals improves. WAXS results also reveal that there is a tilted-orientation of the molecular *c*-axis with respect to the Z-axis of a few degrees (less than 10 °), as discussed by Asano and Seto [2].

Figure 4 illustrates the "through" (left-hand side) and the "edge" (right-hand side) SAXS patterns recorded for the annealed cold-drawn PET samples. The 4-point diagrams shown in Figure 4 suggest the occurrence of an inclined nanolayer packing, in agreement with the previous published work [5]. It is noteworthy the increase in scattered intensity with increasing annealing temperature, in a similar manner as that observed for WAXS (see Figure 3). In addition, the inclination angle, θ, defined as the angle between the normal to the lamellae and the Z-axis, is larger in the edge pattern. Table 1 collects the θ values obtained in the through-, θ_t, and in the edge-surfaces, θ_e, together with the layer spacing values along the Z-axis, L_z. Table 1 also includes the average values of the crystalline layer thickness, l_c, calculated according to;

$$l_c = L_z \, \alpha \cos \theta \tag{7}$$

Equation 7 has been assumed to be valid for $\alpha \geq 0.40$. For $\alpha < 0.40$, the amount of amorphous material outside the lamellar stacks is significant and hence, equation 7 yields l_c values that should be taken as a lower limit to the average crystal thickness of the material (see l_c values in brackets in Table 1).

In summary, crystalline layers of annealed cold-drawn PET samples are characterized by a large inclination angle whereas the crystalline molecules remain nearly parallel to the Z-axis. The mechanism of layer formation is discussed below, as compared to that of hot-drawn PET.

3.1.3. Crystallization of hot-drawn PET upon annealing: comparison with cold-drawn studies

Crystallization of the hot-drawn samples takes place upon annealing at $T_a \geq 100$ °C (see Figure 5), leading to a gradual development of order with increasing T_a in a similar manner as that observed for cold-drawn PET (see Figure 3). However, the following main differences can be distinguished between the WAXS patterns of the crystallized hot- and cold-drawn samples: i) The intensity of each reflection for hot-drawn PET is distributed along an arc, in contrast to the distinct (*hkl*) reflections in case of cold-drawing. This is a consequence of an average lower degree of molecular orientation within the crystals in the hot-drawn sample with respect to the cold-drawn one. ii) The *c*-axis tilting with respect to the Z-axis is substantially larger for the hot-drawn material (≈ 30 °), as compared to that found for the cold-drawn one (< 10 °). For hot-drawn PET at low T_a (100 – 150 °C), the inclination of the (010) plane is about 10 – 15 ° whereas that of the (100) plane is ~ 30 – 40 °. Hence, the average molecular inclination of the triclinic crystal is ~ 30 °. At $T_a = 200$ °C, the (010) and (100) reflections are displaced up and down from the equator by 20 – 25 °, yielding an inclination of the triclinic *c*-axis of about 30 °. Finally, the WAXS patterns at 250 °C exhibit a sharp meridional (001) reflection, indicating that the normal to the triclinic (001) planes is parallel to the Z-axis, and hence, the molecular *c*-axis is tilted about 30 °.

Figure 6 illustrates the SAXS patterns for various annealed hot-drawn PET samples. Two-point patterns are clearly displayed for T_a = 100 °C and 250 °C, indicating that the normal to the layer surface is parallel to the Z-direction. For T_a = 150 °C and 200 °C, a small θ value is observed. Table 1 collects the L_z, θ_t, θ_e, and l_c ("through" and "edge", calculated using equation 7) values obtained from the analysis of the SAXS patterns of Figure 6.

Figure 7 (bottom) illustrates the L_z and l_c ("edge" and "through") variation with T_a for hot-drawn PET. Data for cold-drawn PET, for both the through- and the edge-surfaces, have been included in Figure 7 (top) for comparison. It is noteworthy the l_c increase with increasing T_a for both, hot- and cold-drawing. For hot-drawing, the l_c values in the "edge" and "through" directions lie within the experimental error, while slightly larger values are found for l_c "through" in case of the cold-drawn material.

The above WAXS and SAXS results for cold- and hot-drawn PET are schematically summarized in Figure 8. For cold-drawing, molecules within the crystalline layers remain nearly parallel to the Z-axis while the lamellae exhibit a large inclination angle (18 ° ≤ θ ≤ 53 °). A gradual increase of T_a leads to larger l_c values and at the same time the layer inclination angle decreases. In addition, slightly larger l_c and smaller θ values are found in the "through" direction. In case of hot-drawing, molecules within the crystalline layers are largely inclined with respect to the drawing axis (~30 °), while the lamellar inclination angle remains nearly parallel to the Z-direction (θ < 15 °). Similar l_c values are found in the "through" and in the "edge" directions, both increasing as T_a is raised.

In Figure 9, the WAXS end patterns for, both, the cold- and the hot- drawn samples annealed at 250 °C are compared. The intensity distribution along the diffraction rings of Figure 9 (a) suggests that PET crystals exhibit a biaxial orientation in the cold drawn sample, where the crystalline *c*-axis is parallel to the Z-axis, and the (100) plane (or the crystalline *b*-axis) is parallel to the film surface. The degree of biaxial orientation increases with increasing annealing temperature (results not shown here), up to the extent shown in Figure 9a, for the range of T_a considered.

The biaxial orientation in case of cold-drawing is a consequence of the cross-section of the PET molecule: the flat-shaped benzene rings of highly oriented molecules are apt to align with the film surface. Upon crystallization at increasingly high temperatures, the (100) plane moves towards the Y-axis. The occurrence of biaxial orientation could clarify the differences found between the inclination of the layers in the "through" and "edge" arrangements (see Table 1). Assuming that the layer surface coincides with the (001) plane, then, the fact that the *c*-axis is not perpendicular to this plane ($\alpha = 98.5$ ° and $\beta = 118$ ° for the triclinic crystal structure of PET), would explain the θ_t - θ_e values approaching β - $\alpha = 10$ °.

In case of the hot-drawn sample, the end pattern in Figure 9(b) has a uniform distribution of intensity along the diffraction rings in the XY plane. This fact indicates that the material exhibits a uniaxial orientation. As a result, no difference is found between the lamellar inclination angles for the 'through' and 'edge' X-ray patterns.

3.1.4. Layer formation mechanism

In our preceding studies, the crystallization mechanism for cold-drawn PET was explained via a tilting mechanism, giving rise to inclined surface layers [2, 5]. Starting from the highly oriented paracrystalline (nematic or smectic) state, the phase separation into crystalline and amorphous layers is promoted by a slight inclination, δ, of the molecular axis. Figure 10a (left-hand side) schematically illustrates the different average molecular distance in the crystalline and in the nematic layers, d_c and d_a respectively, arising from a small inclination of the molecules with respect to the Z-direction, δ. In our preceding studies, we already highlighted the fact that a small δ–value ($\delta = 1$ °) would already yield a significant density difference between the crystalline and the amorphous layers [5]. The average density difference between the crystalline and the amorphous layers can be calculated following [5]:

$$\rho_c/\rho_a = d_a / d_c = d \sin\delta_a / d \sin\delta_c = \sin\delta_a / \sin\delta_c \qquad (7)$$

where d is the molecular distance along the layer surface (see Figure 10a), and δ_a and δ_c are defined as the angles between molecules in the amorphous and crystalline layers and the inclined layer surface, respectively (see Figure 10a). Using ρ_c = 1.455 g/cm^3 and ρ_a = 1.37 g/cm^3, $\sin\delta_a / \sin\delta_c$ = 1.062 [5].

On the other hand, the layer inclination angle θ and the average inclination of the crystalline and amorphous layers δ are directly related through (see Figure 10a):

$$(90\,^\circ - \theta) + \delta + \delta_a = 180\,^\circ$$
$$(90\,^\circ + \theta) + \delta + \delta_c = 180\,^\circ \qquad (8)$$

Combination of equation 8 with $\sin\delta_a / \sin\delta_c = 1.062$ yields:

$$\delta = \text{artg}\left[\frac{0.0301}{\tan\theta}\right] \qquad (9)$$

Equation 9 permits the anticipation of the c-axis tilting values based on the values of the lamellar inclination. Table 2 collects the δ values obtained using equation 9, assuming a series of θ values close to the ones reported for cold-drawn PET at different T_a (see Table 1). In all cases, a small value of δ is found, in the range of those measured experimentally (< 10 °).

Equation 9 is of great significance because it highlights the intimate interrelationship between δ and θ: the larger is the layer inclination, the smaller is the molecular inclination necessary to induce the required density difference between the crystalline and the amorphous phases. Equation 9 can be extended for hot-drawn PET. In Table 2, the θ values ≤ 10 ° give rise to $\delta \geq 10$ °, in agreement with the experimental results for hot-drawing. Hence, we conclude that the layer structure formation involves a supplementary relationship between δ and θ.

In view of the above considerations we envisage the mechanism of layer formation in cold-drawn PET as promoted by a slight inclination of the molecules in the nematic state, giving rise to an inclined layer surface. At low annealing temperatures, the molecular inclination is the lowest ($\delta < 2$ ° for T_a = 100 °C) and the lamellar inclination the largest ($\theta = 53$ ° for T_a = 100 °C). Increasing the annealing temperature leads to thicker crystalline layers with slightly larger c-axis

tilting as a consequence of the relaxation of the oriented molecules ($\theta = 20$ ° for $T_a = 250$ °C; $\delta \approx 5$ °), as schematically depicted in Figure 10a (right-hand side).

In contrast to cold-drawn PET, the hot-drawn material exhibits a low degree of molecular orientation, as mentioned above. During crystallization, the disordered segments should be rejected from the developing crystalline layers. For hot-drawing, due to the lower degree of molecular orientation, molecules are allowed to adopt a larger number of molecular conformations than those in the highly oriented sample. This would facilitate, not only the occurrence of molecular foldings at the crystal surface and within the amorphous layers, but also the matching of neighbouring chains with a certain tilting angle with respect to the draw direction. Molecular foldings would enhance the density difference between the crystalline and the amorphous regions, hence, reducing the extent of the molecular inclination angle necessary for crystallization. The molecular *c*-axis tilting found in the hot-drawn crystal emerges as a consequence of the need to reduce the average molecular distance within the crystalline layers with respect to the non-crystalline ones. As a result, crystallization of hot-drawn PET gives rise to surface nanolayers perpendicular to the draw direction (see Figure 10b). The local molecular orientation within the amorphous layers should be randomly distributed, with an average chain direction parallel to the Z-axis (straight dotted line in Figure 10b).

3.2. Microhardness Measurements

3.2.1 Comparison of cold drawing and hot drawing

Fig. 11 (top) illustrates the microhardness values measured perpendicular to the draw direction (top), $H_\perp$, and the corresponding indentation anisotropy values (bottom) for the cold-drawn and hot-drawn samples. The $H_\perp$ values of the cold-drawn sample fit very well with previous published data [5]. Results show that $H_\perp$ is larger for the hot-drawn than for the cold-drawn samples.

However, this difference gradually diminishes with increasing T_a, and both $H_\perp$ values coincide for $T_a = 250$ °C.

Most interesting is the fact that, while the indentation anisotropy in case of the cold-drawn material decreases with T_a above T_g, in case of hot-drawing, ΔH is practically zero for all the samples (see Fig 11 bottom). The cold-drawn ΔH data also fit satisfactorily with our previous published work [5]. The fact that $\Delta H \approx 0$ for the hot-drawn samples and the cold-drawn ones annealed at the highest temperature, while the WAXS and SAXS patterns reveal a significant degree of orientation, suggests that ΔH is governed by the elastic response of the molecules located within the amorphous regions. Indeed, the ΔH conspicuous decrease above $T_a \approx 70$ °C for the cold-drawn material has been previously associated to a relaxation mechanism of the molecules in the amorphous layers. As a result, elastic recovery in the chain direction decreases, and hence, ΔH diminishes.

For the un-annealed material, the large difference in microhardness and ΔH between cold- and hot-drawn PET appears to be mainly due to the different degree of molecular orientation (see Figure 2), the more oriented material yielding lower $H_\perp$ values. In the cold-drawn material, the plastic deformation induced by the indentation in the direction perpendicular to the drawing is mainly due to the separation of molecules bound by van der Waals forces. In contrast, in the hot-drawn material, owing to the lack of good orientation, intramolecular covalent forces may also contribute to the microhardness value. In addition, a slight initial crystallization may as well play a role in the microhardness enhancement for hot-drawing.

Let us recall that the initial $H_\perp$ increase with T_a for the cold-drawn samples within the interval 25 °C < T_a < 100 °C was associated to the gradual appearance of smectic domains with increasing degree of perfection, and the development of crystallinity at $T_a \geq 80$ °C [5]. At $T_a \geq 100$ °C, only the triclinic crystallization takes place and the hardness increase with increasing T_a for both, hot- and cold-drawn, is directly related to the gradual rise in crystallinity and crystal thickness (see Table 1 and Fig. 7). Moreover, the hardness difference between the hot-drawn and the cold-drawn samples

for $T_a \geq 100$ °C is also mainly related to changes in the developing nanostructure. Indeed, the H values for both series can be accounted for by introducing the corresponding α and l_c values (see Table 1) in equations 4 and 5 ($H_\perp^\infty = 358$ MPa; $H_a = 140$ MPa; $b = 1 - 8$ nm [5, 17-19, 22]). A detailed discussion on the influence of the b-parameter on the H-values is given below.

3.2.2. Influence of the layer surface on microhardness

In previous studies, we investigated the b-parameter for various PET materials and values of b in the range of 1 – 8 nm were obtained [17-19, 22]. The value of b has been related to the surface perfection of the crystals and modulates accordingly the hardness values. For the calculation of b (using equations 4 and 5), we have assumed a $H_\perp^\infty$ value of 358 MPa and $H_a = 140$ MPa, which are both derived for oriented PET [5]. Figure 12 illustrates the variation of the b-parameter with T_a, for the hot-drawn and the cold-drawn samples. It is seen that the small difference found between the b-values for hot- and cold-drawing lies within the experimental error. The notable increase of b at $T_a = 250$ °C resemble the sudden increase of b obtained for isotropic PET samples at $T_a = 240$ °C [22]. In that case, the b-rise has been ascribed to the decrease of Δh due to a chain scission process occurring at high temperature that could result in: i) a reduction of entanglements within the amorphous intercrystalline layers and ii) a decrease of tie molecules connecting adjacent lamellae [5].

3.2.3. Microhardness measurements on the film- and along the edge-surface

Fig. 13 comparatively illustrates the microhardness variation with T_a, for the cold-drawn (bottom) and the hot-drawn (top) samples measured on the edge-surface, $H_\perp^{edge}$, and on the film surface, $H_\perp$ (results also shown in Fig. 11). It is to be noted that, for cold and hot drawn samples, $H_\perp^{edge}$ is always smaller than $H_\perp$ and both values increase with temperature, similarly as in Fig. 11.

It is noteworthy that indentation anisotropy values on the film surface and on the edge (not shown here) are within the error of measurement for both, cold- and hot-drawn samples.

As discussed above, the biaxial orientation found in cold-drawn PET results in a different lamellar inclination in the "through" and "edge" SAXS 4-point patterns. However, it is difficult to explain the difference between $H_{\perp}$ and $H_{\perp}^{edge}$ in the light of the observed structural variations. Moreover, the crystal thickness values obtained for the measurements "through" and "edge" of the cold-drawn material (see Table 1) would only yield a hardness difference of about 1% (see equation 5). On the other hand, no significant variations between the "through" and the "edge" x-ray diffraction measurements have been discussed so far in case of hot-drawing. However, a closer inspection of the SAXS patterns of the cold- and the hot-drawn material (Figures 4 and 6) reveals the appearance of an equatorial continuous scattering. The occurrence of this scattering indicates the presence of microvoids (provoking a great density difference) which could act as weak zones during the indentation measurement. Hence, the slightly lower $H_{\perp}^{edge}$ values with respect to $H_{\perp}$ can be attributed to the occurrence of microvoids.

4. Conclusions

1. Hot-drawing of glassy PET yields a material with a lower degree of molecular orientation than cold-drawing.

2. Crystallized cold-drawn PET exhibits a biaxial orientation normal to the lamellae surface, in contrast to the uniaxial orientation found for crystallized hot-drawn PET.

3. In the cold-drawn material, the triclinic *c*-axis is slightly tilted, and the normal to the lamellar surface is largely inclined with respect to the drawing direction (4-point SAXS pattern). In contrast, in case of hot-drawn PET, the molecular *c*-axis is largely tilted with respect to the Z-axis and the lamellar normal remains nearly parallel to the Z-axis (2-point pattern).

4. A mutual supplemental relationship is found between the inclination angle of the lamellae and the *c*-axis tilting. In cold-drawn PET, a conspicuous lamellar inclination is necessary to produce a significant density difference between the crystalline and the non-crystalline domains. In this case, the lamellar surface is largely inclined. For hot-drawing, due to a lower degree of molecular orientation, molecules may adopt a larger number of molecular conformations. Hence, a large molecular inclination is induced upon crystallization, leading to the formation of stacks of flat layers (lamellae surface perpendicular to Z-axis).

5. A large difference is found between the $H_{\perp}$ values of the un-annealed cold- and hot-drawn samples due to the occurrence of a higher molecular orientation in the former.

6. The increase in the degree of crystallinity and crystal thickness with increasing T_a gives rise to a parallel increase in $H_{\perp}$, for, both, hot-drawn and cold-drawn samples. In addition, the differences in hardness found between hot and cold-drawing can be also explained in terms of crystallinity and crystal thickness.

7. For cold-drawn samples, the indentation anisotropy ΔH decreases with T_a (for $T_a \geq T_g$) leading to ΔH values converging to those for the hot-drawn material ($\Delta H \approx 0$). The fact that the WAXS and SAXS patterns at high temperature reveal a significant degree of orientation for the cold-drawn material, suggest that ΔH is governed by the elastic response of the molecules located within the amorphous regions.

8. The smaller hardness values found on the edge surface with respect to those measured on the film surface are ascribed to the occurrence of microvoids as revealed by the appearance of continuous equatorial scattering in the SAXS patterns.

Acknowledgements

Grateful acknowledgement is due to the MEC, Spain (grant FIS2004-01331) for the generous support of this work.

References

1. Göschel U. Polymer 1995;36:1157.
2. Asano T, Seto T. Polym J 1973;5(1):72.
3. Bonart R. Kolloid-Z. 1966;1:213.
4. Yeh GSY, Geil PHJ. J Macromol Sci Phys 1967;B1:235.
5. Asano T, Baltá Calleja FJ, Flores A, Tanigaki M, Mina MF, Sawatari C, Itagaki H, Takahashi H, Hatta I. Polymer 1999;40:6475.
6. Nicholson TM, Davies GR, Ward IM. Polymer 1994;35:4259.
7. Welsh GE, Blundell DJ, Windle AH. Macromolecules 1998;31:7562.
8. Kawakami D, Ran S, Burger C, Fu B, Sics I, Chu B, Hsiao BS. Macromolecules 2003;36:9275.
9. Kawakami D, Hsiao BS, Ran S, Burger C, Fu B, Sics I, Chu B, Kikutani T. Polymer 2004;45:905.
10. Elsner G, Koch MHJ, Bordas J, Zachmann HG. Makromol Chem 1981;181:1263.
11. Elsner G, Riekel C, Zachmann HG. Adv Polym Sci 1985;1:67.
12. Günter B, Zachmann HG. Polymer 1983;24:1008.
13. Asano T, Zdeick-Pickuth A, Zachmann HG. J Mater Sci 1989;24:1967.
14. Santa Cruz C, Stribeck N, Zachmann HG, Baltá Calleja FJ. Macromolecules 1991;24:5980.
15. de Daubeny PR, Bunn CW, Brown CJ. Proc Roy Soc 1954;226:531.
16. Baltá Calleja FJ, Fakirov S. The microhardness of polymers. Cambridge: Cambridge Univ Press, 2000.
17. Santa Cruz C, Baltá Calleja FJ, Zachmann HG, Stribeck N, Asano T. J Polym Sci Polym Phys 1991;B29:819.
18. Baltá Calleja FJ, Baranowska J, Rueda DR, Bayer RK. J Mater Sci 1993;28:6074.
19. Baltá Calleja FJ, Öhm O, Bayer RK. Polymer 1994;35:4775.
20. Baltá Calleja FJ, Santa Cruz C, Asano T. J Polym Sci Polym Phys 1993;31:557.
21. Flores A, Baltá Calleja FJ. Phil Mag 1998;A78:1283.

22. Flores A, Pieruccini M, Stribeck N, Funari SS, Bosch E, Baltá Calleja FJ. Polymer 2005;46:9404.

23. Göschel U, Deutscher K, Abetz V. Polymer 1996;37:1.

Table 1. Lamellar spacing along the draw direction, L_z; lamellar inclination angle with respect to the 'through', θ_t, and the 'edge' directions, θ_e; degree of crystallinity, α; crystal lamellar thickness in the "through", $L_z\alpha\cos\theta_t$, and in the "edge", $L_z\alpha\cos\theta_e$, directions; for cold-drawn and hot-drawn PET annealed at various temperatures T_a for 10^4 s.

T_a (°C)	L_z (nm)	θ_t (°)	θ_e (°)	α	$L_z\alpha\cos\theta_t$ (nm)	$L_z\alpha\cos\theta_e$ (nm)
Cold-drawn PET						
100	10.7	52	53	0.22	(1.5)	(1.4)
150	11.2	41	49	0.39	3.3	2.9
200	12.6	34	39	0.55	5.8	5.4
250	16.4	18	26	0.80	12.5	11.8
Hot-drawn PET						
100	11.2	0	0	0.40	4.5	4.5
150	10.5	7	9	0.51	5.3	5.3
200	11.2	14	12	0.67	7.3	7.3
250	13.7	0	0	0.91	12.5	12.5

Table 2. Values of the angle of molecular tilting, δ, obtained using Equation 9, as a function of the inclination of the layer surface, θ (assuming $\rho_c / \rho_a = 1.062$, see text).

θ (°)	δ (°)
Cold-drawn PET	
50	1.5
40	2.0
30	3.0
20	4.7
Hot-drawn PET	
10	9.7
5	19
3	30

FIGURE CAPTIONS

Figure 1. Coordinates of the drawn PET sample. Schematics of the "through" and the "edge" arrangements.

Figure 2. (a) WAXS pattern of the un-annealed cold- (left-hand side) and hot- (right-hand side) drawn sample (b) azimuthal scan of the intensity distribution at $2\theta = 20 \pm 2$ °, for the un-annealed cold-drawn (dotted line) and hot-drawn (solid line) PET sample.

Figure 3. WAXS patterns of cold drawn PET annealed at various T_a for 10^4 s, taken in the "through" (left-hand side) and in the "edge" (right-hand side) arrangements.

Figure 4. SAXS patterns, in the "through" (left-hand side) and in the "edge" (right-hand side) direction, of cold drawn PET annealed at various T_a for 10^4 s.

Figure 5. WAXS patterns of hot-drawn PET annealed at various T_a for 10^4 s, taken in the "through" (left-hand side) and in the "edge" (right-hand side) arrangements.

Figure 6. SAXS patterns of hot-drawn PET, in the "through" (left-hand side) and in the "edge" (right-hand side) direction, annealed at various T_a for 10^4 s.

Figure 7. Lamellar spacing along the draw direction (■), and crystal layer thickness values in the "through" (▽) and in the "edge" (▲) directions, for cold-drawn (top) and hot-drawn (bottom) PET, as a function of T_a.

Figure 8. Schematics of the layer profiles for cold- and hot-drawn PET developing at different T_a. In case of cold-drawing, a different layer profile has been drawn for the "through" and the "edge" directions. For the sake of simplicity, the molecular direction has been schematically represented by one single molecule in the layer profile corresponding to the highest T_a.

Figure 9. WAXS end patterns of the cold- and hot-drawn samples annealed at 250 °C.

Figure 10. Schematic representation of the molecular tilting (δ) and the surface layer inclination (θ) for: a) cold-drawn PET annealed at low and high T_a (left- and right-hand side respectively); b) hot-drawn PET.

Figure 11. Variation of microhardness (top) and indentation anisotropy (bottom) values for cold-drawn (○) and hot-drawn (Δ) PET with annealing temperature. The dotted lines are guides to the eyes.

Figure 12. The *b*-parameter for cold-drawn (○) and hot-drawn (Δ) PET, as a function of T_a.

Figure 13. Microhardness values on the film- (open symbols) and on the edge-surface (solid symbols) for the cold-drawn (○, ●) and the hot-drawn (Δ, ▲) samples, versus T_a.

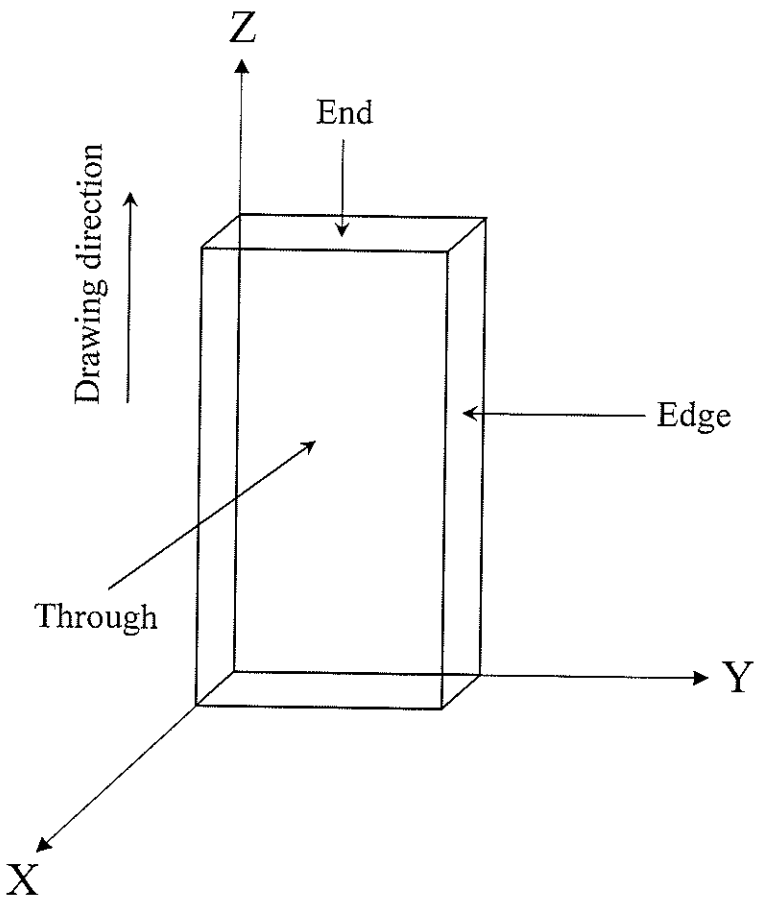

FIGURE 1

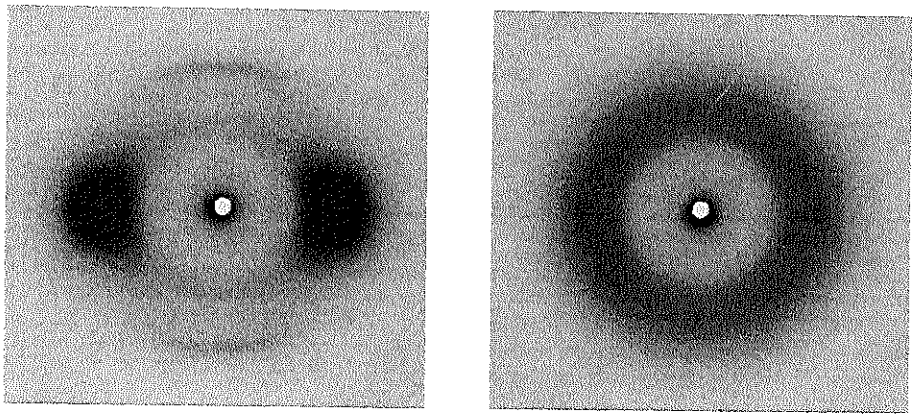

(a)

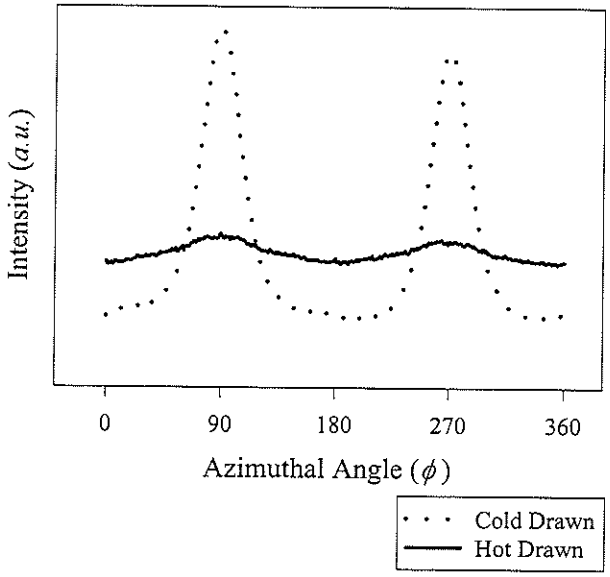
Intensity (a.u.)
0
90
180
270
360
Azimuthal Angle (ϕ)
Cold Drawn
Hot Drawn

(b)

FIGURE 2

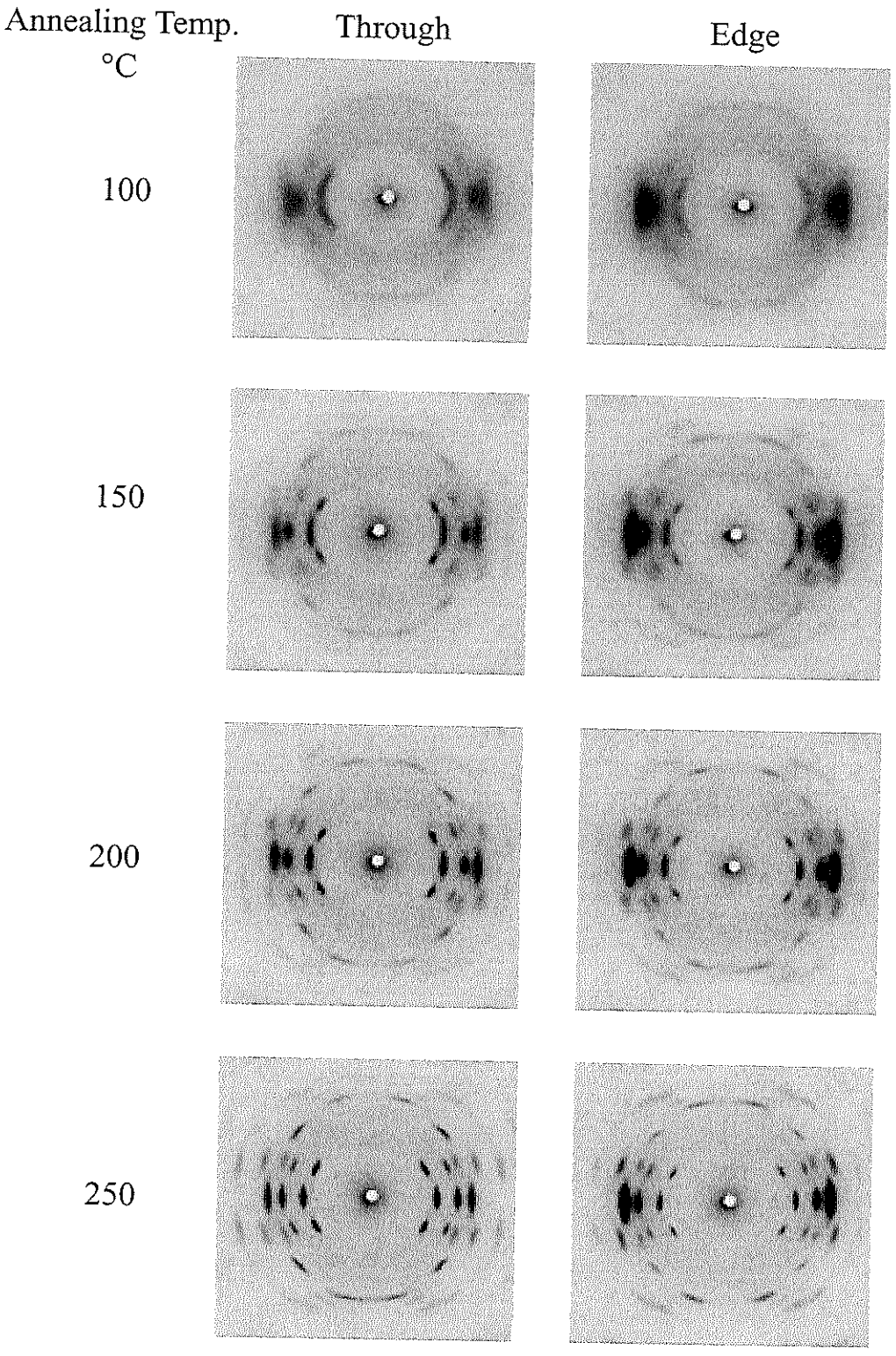

FIGURE 3

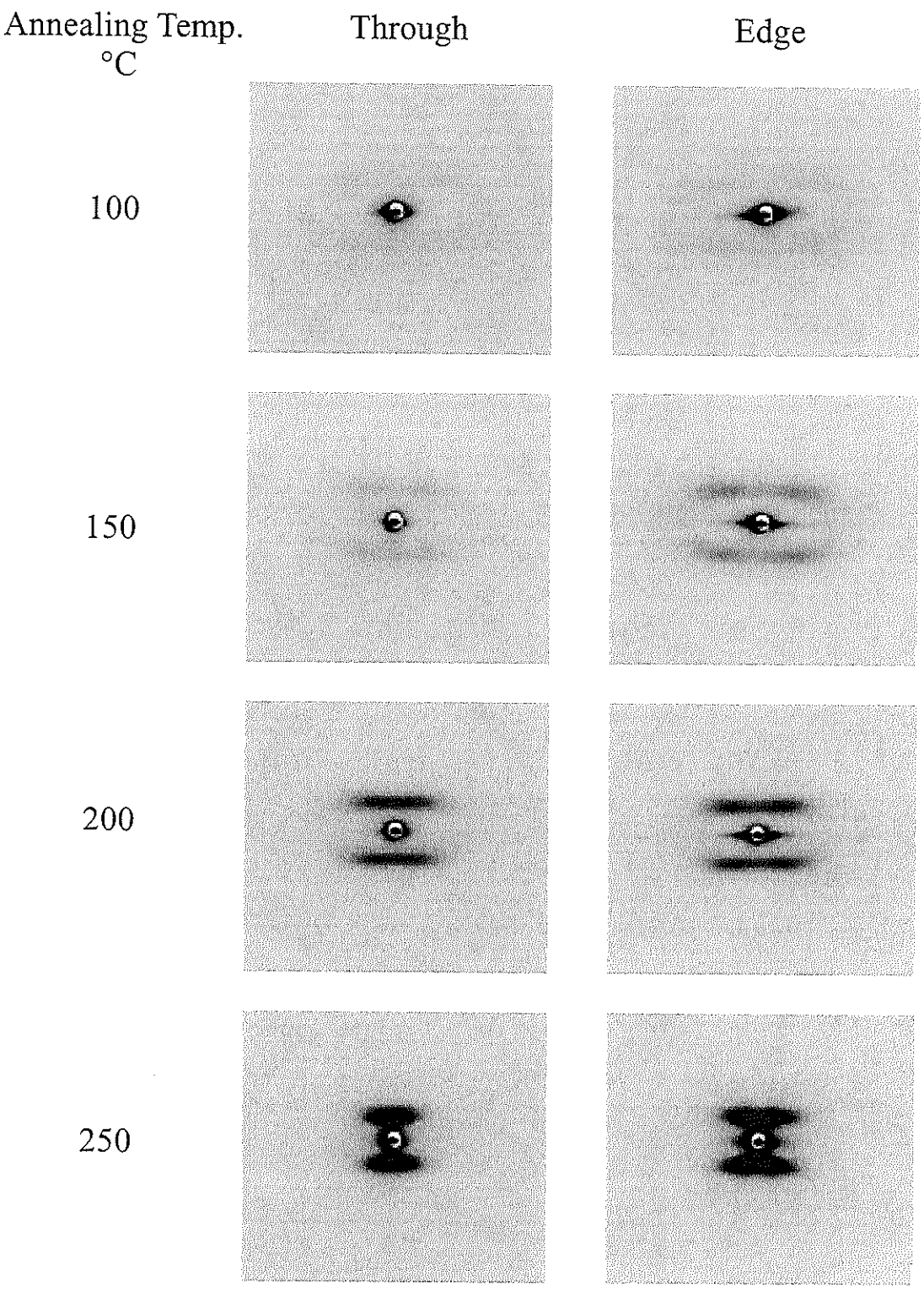

FIGURE 4

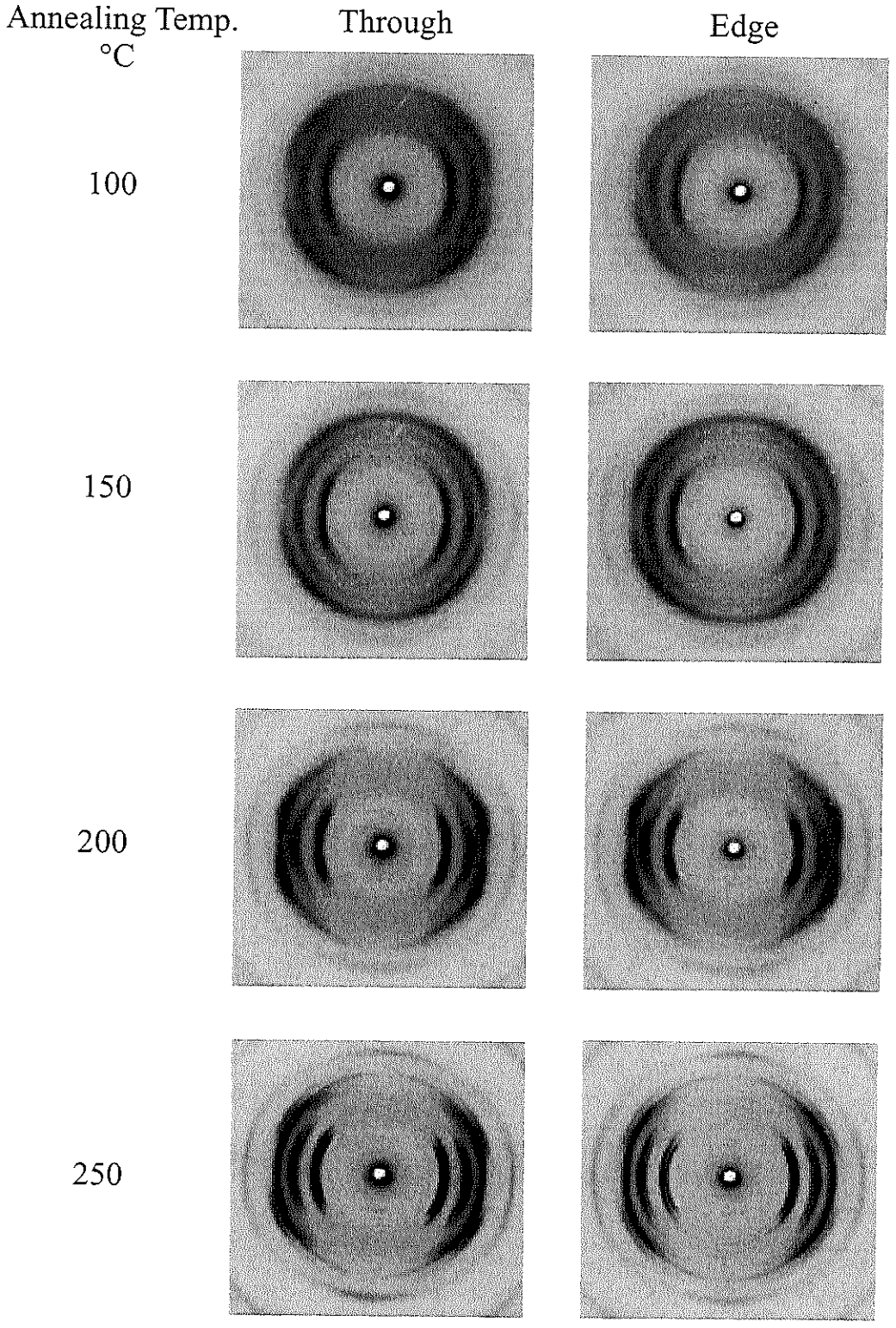

FIGURE 5

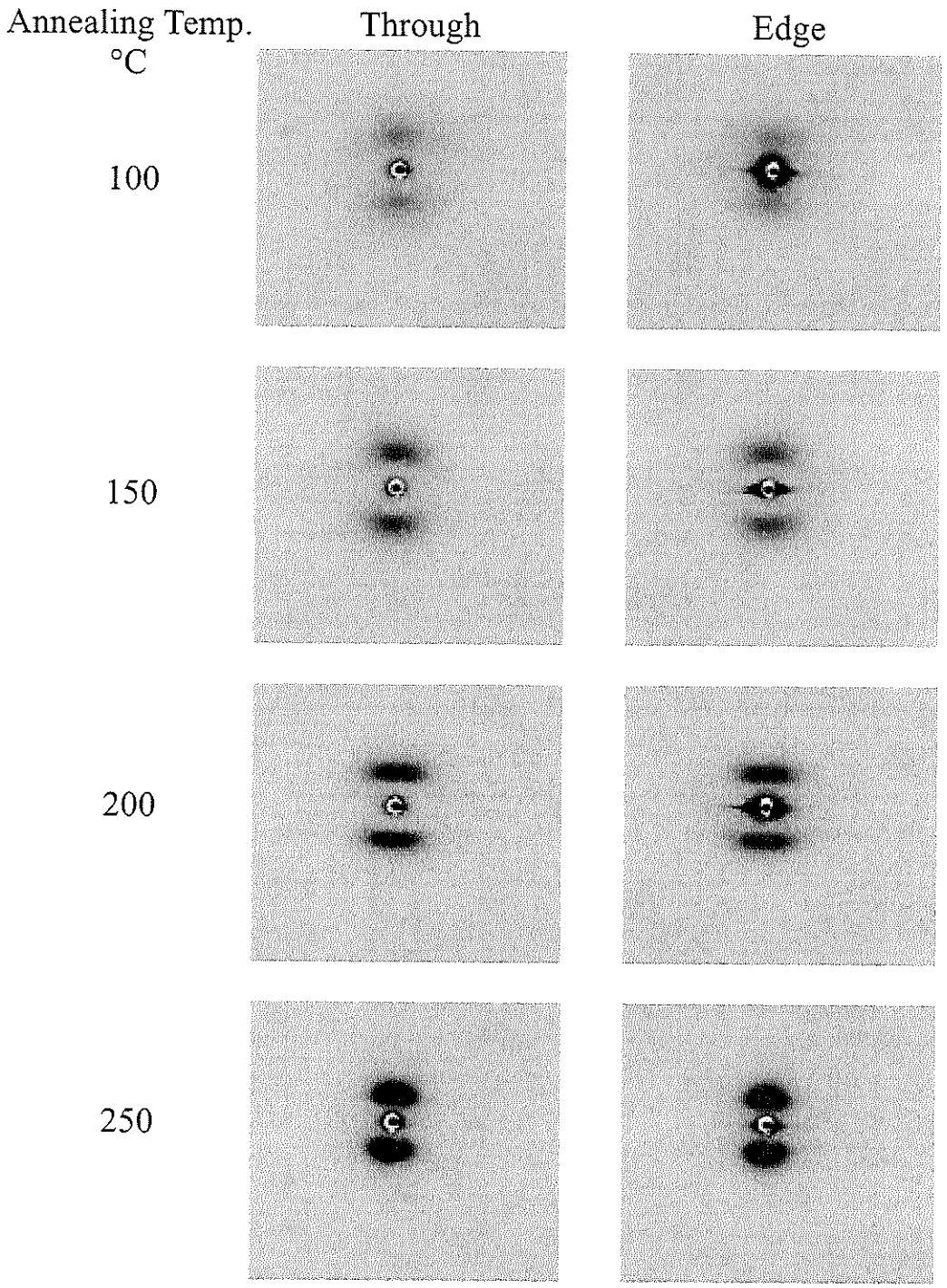

FIGURE 6

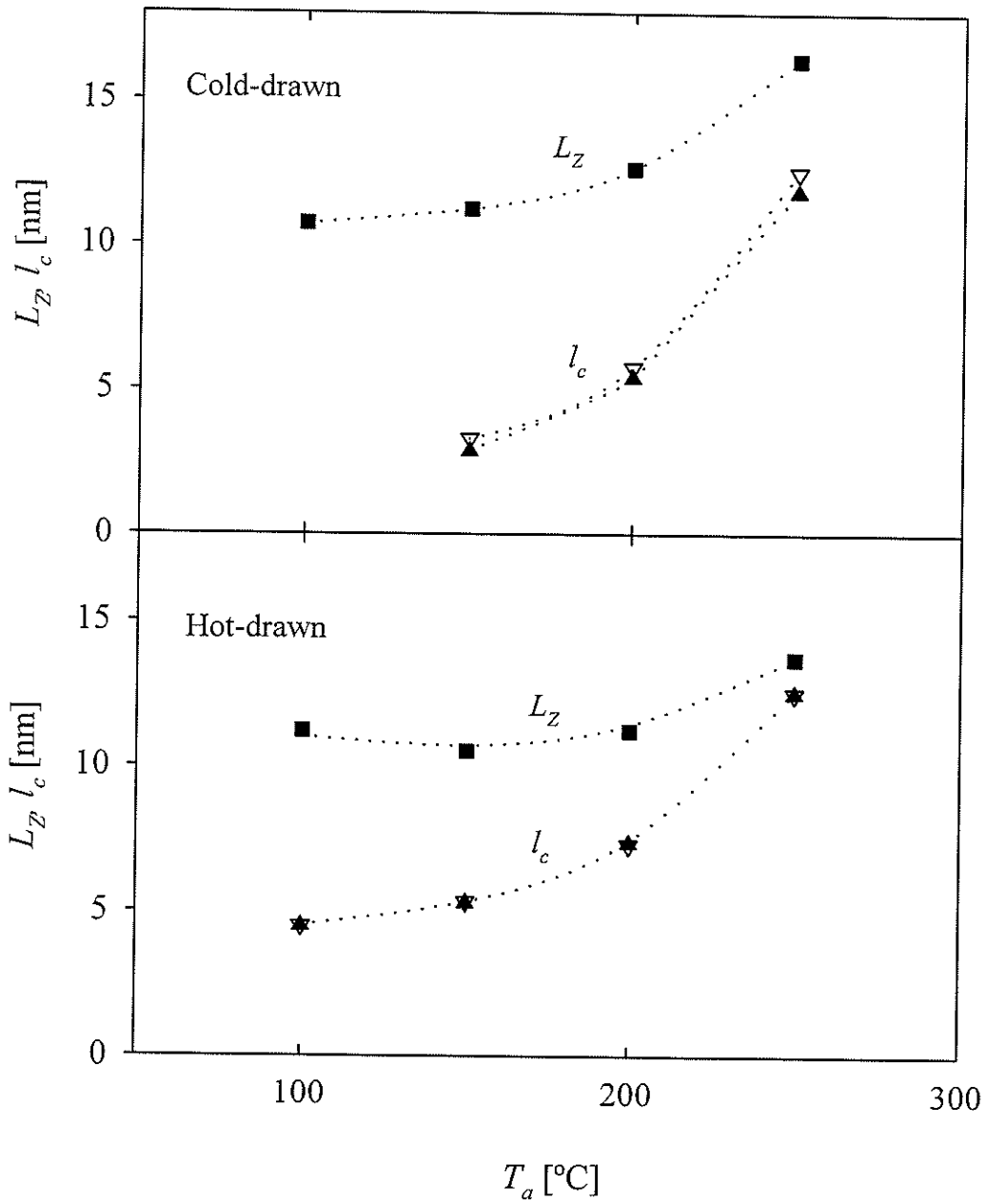

FIGURE 7

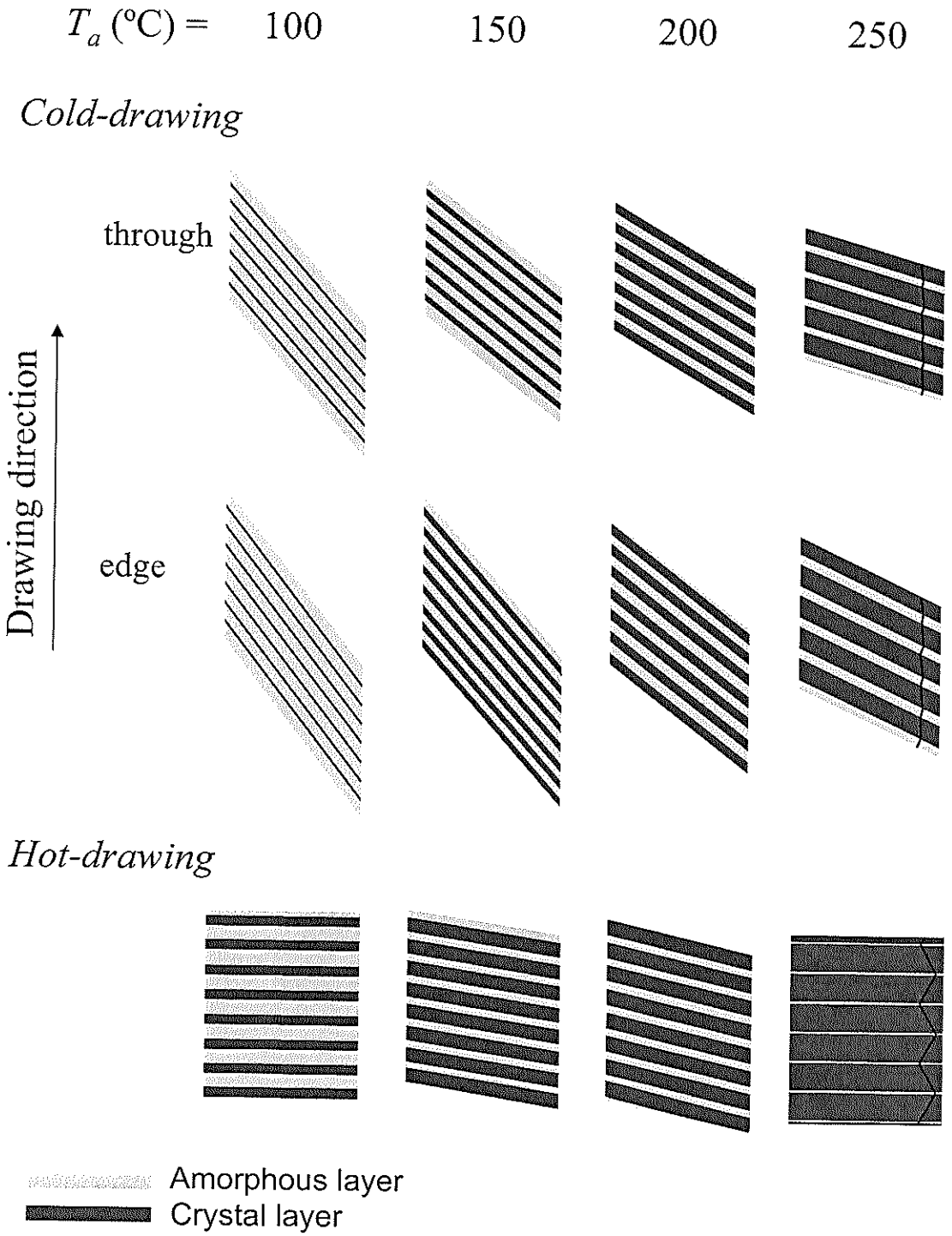
T_a (°C) = 100 150 200 250
Cold-drawing
through
Drawing direction
edge
Hot-drawing
Amorphous layer
Crystal layer

FIGURE 8

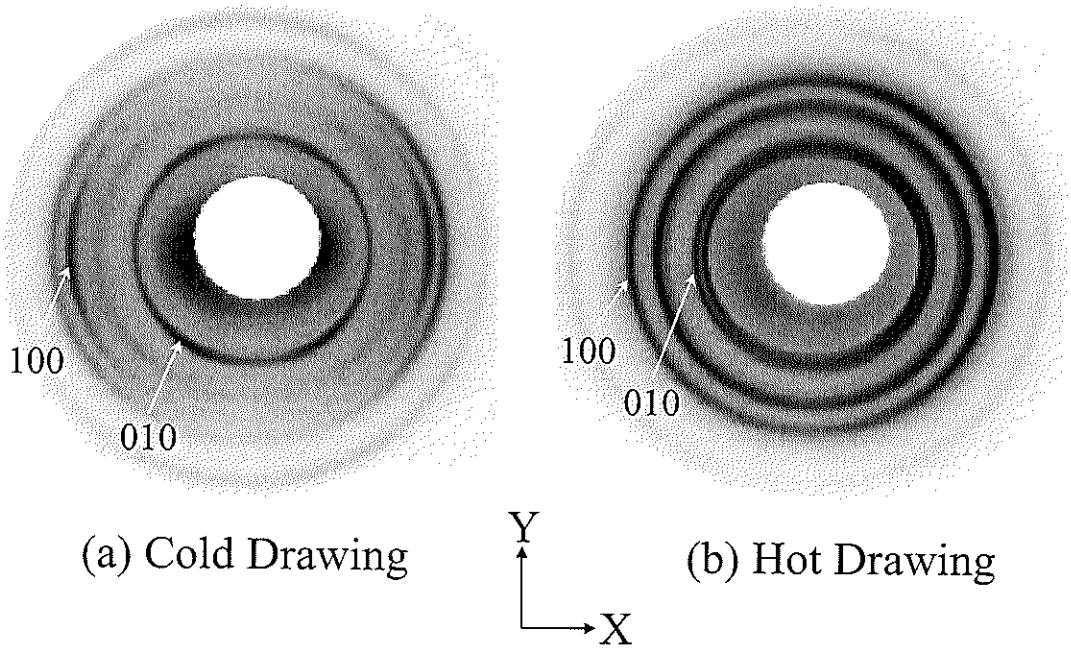

FIGURE 9

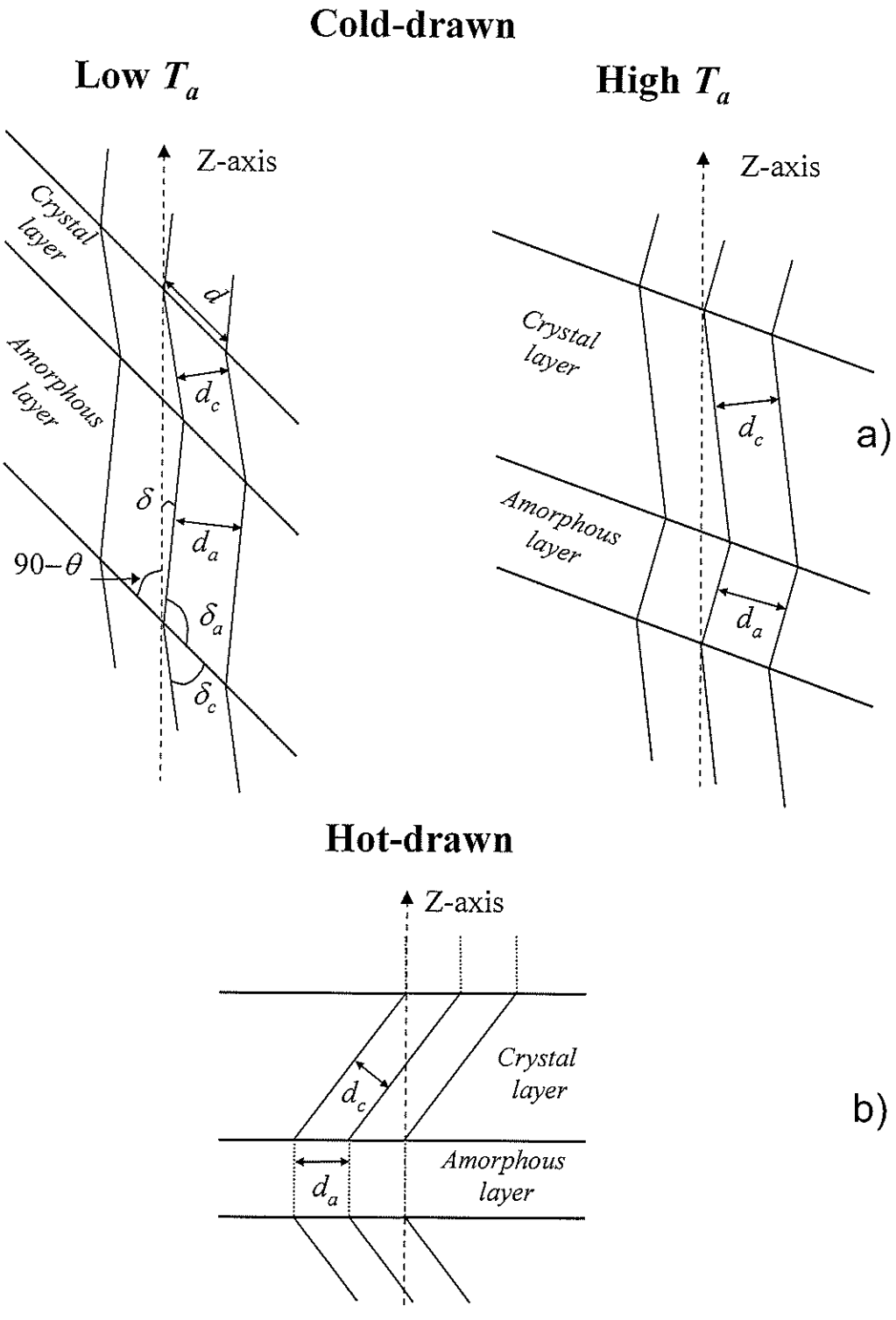
Cold-drawn
Low T_a
High T_a
Z-axis
Crystal layer
Amorphous layer
d
d_c
δ
d_a
90−θ
δ_a
δ_c
a)
b)

FIGURE 10

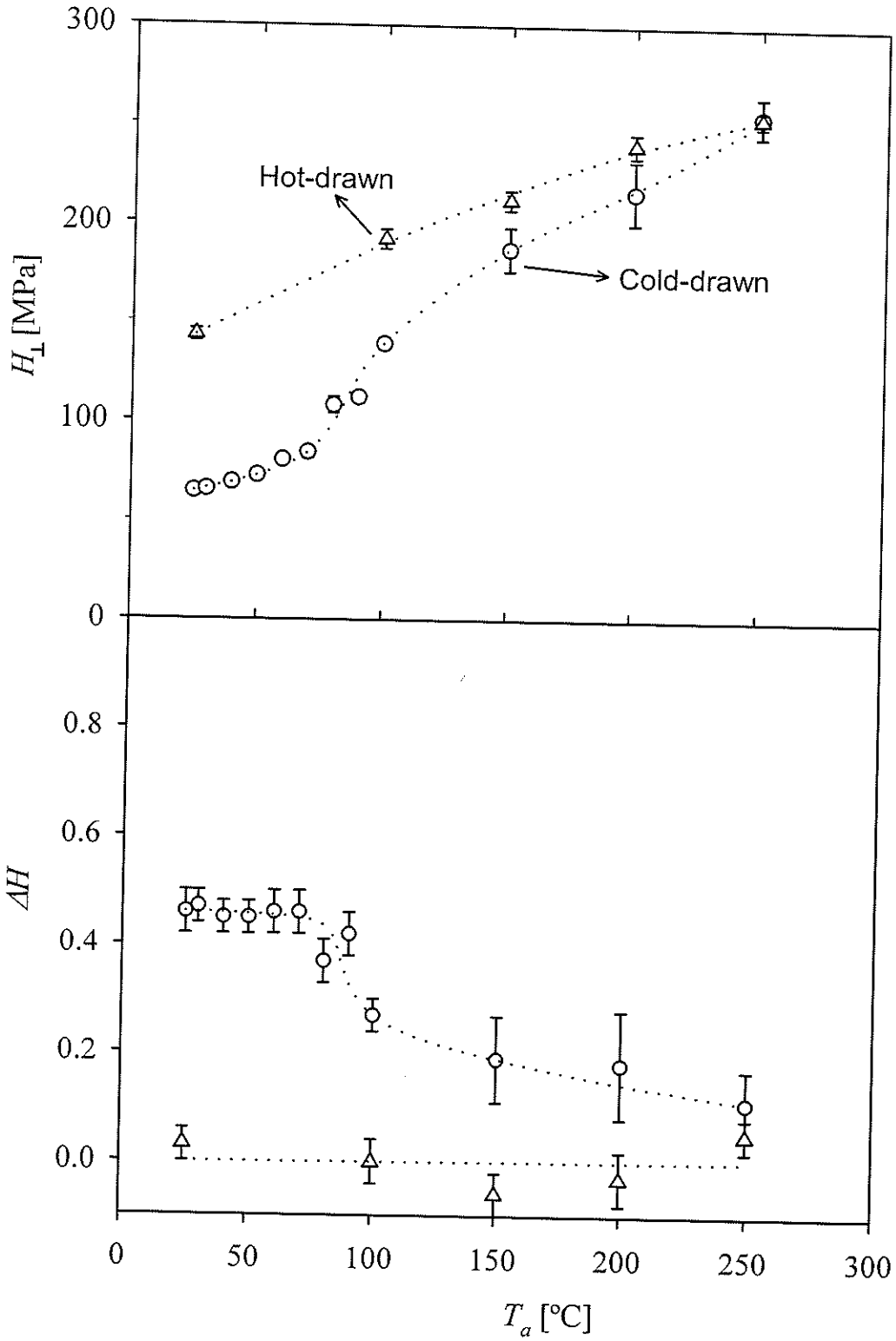
300
200
100
0
$H_\perp$ [MPa]
Hot-drawn
Cold-drawn
0.8
0.6
0.4
0.2
0.0
ΔH
0
50
100
150
200
250
300
T_a [°C]

FIGURE 11

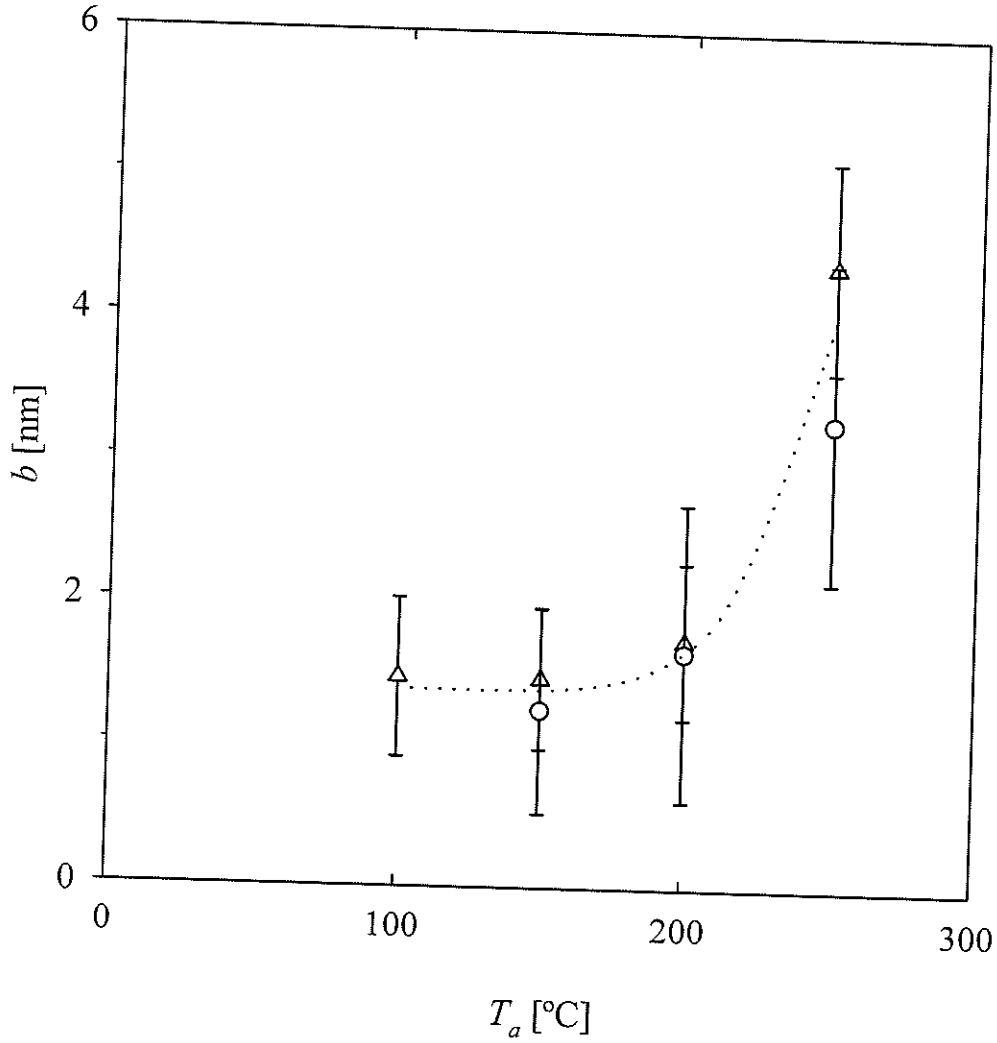

FIGURE 12

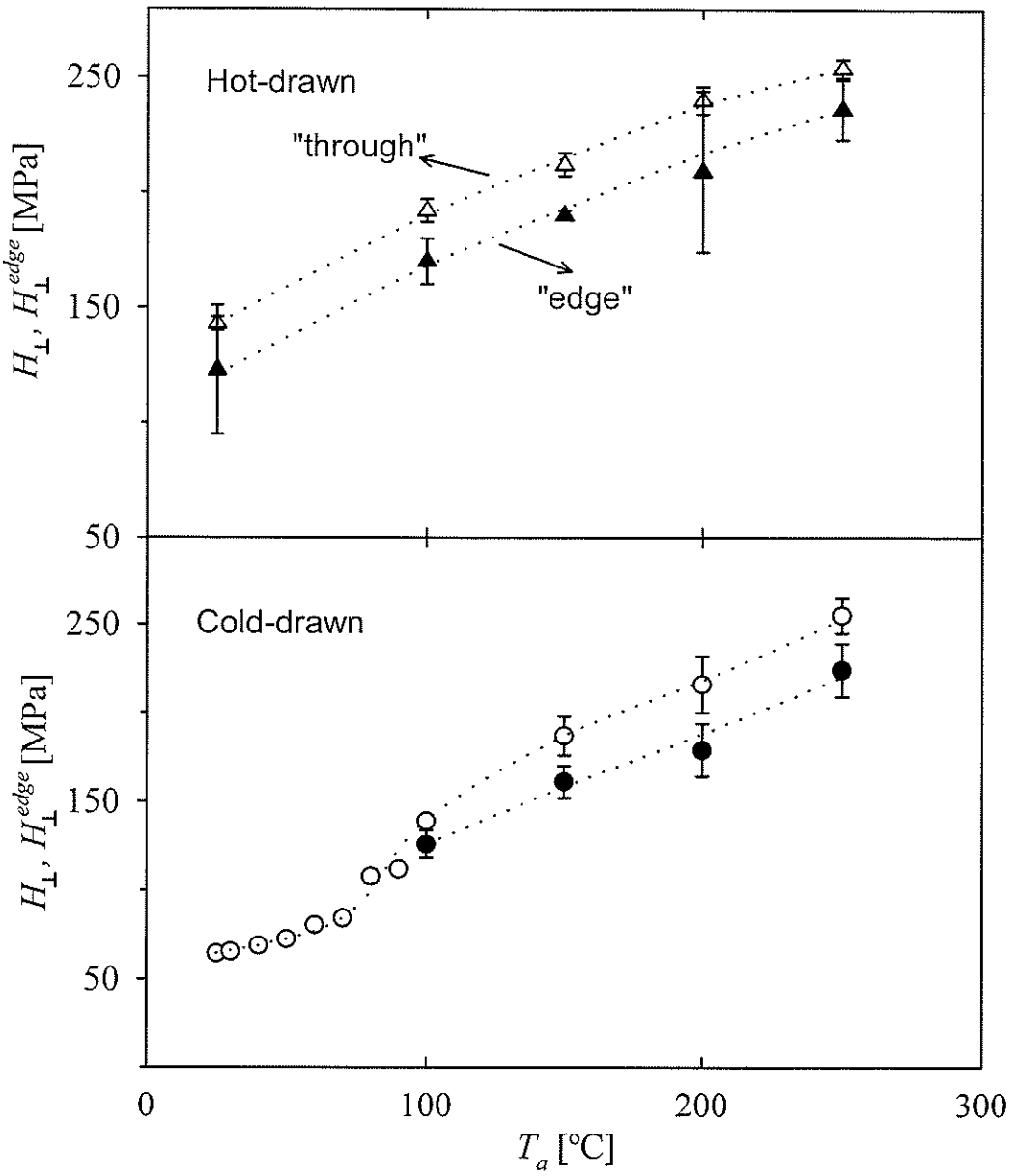
Hot-drawn
"through"
"edge"
Cold-drawn
250
150
50
$H_\perp$, $H_\perp^{edge}$ [MPa]
0
100
200
300
T_a [°C]

FIGURE 13